Nonnormal Amplification of the Thermohaline Circulation

LAURE ZANNA

Department of Earth and Planetary Sciences, Harvard University, Cambridge, Massachusetts

ELI TZIPERMAN

Division of Engineering and Applied Sciences, and Department of Earth and Planetary Sciences, Harvard University, Cambridge, Massachusetts

(Manuscript received 10 September 2004, in final form 1 March 2005)

ABSTRACT

A simple zonally averaged coupled ocean–atmosphere model, with a relatively high resolution in the meridional direction, is used to examine physical mechanisms leading to transient amplification of thermohaline circulation (THC) anomalies. It is found that in a stable regime, in which small perturbations eventually decay, there are optimal initial conditions leading to a dramatic amplification of initial temperature and salinity anomalies in addition to the THC amplification. The maximum amplification occurs after about 40 years, and the eventual decay is on a centennial time scale. The initial temperature and salinity anomalies are considerably amplified by factors of a few hundreds and 20, respectively. The initial conditions leading to this amplification are characterized by mutually canceling initial temperature and salinity anomalies contributions to the THC anomaly, such that the initial THC anomaly vanishes. The mechanism of amplification is analyzed and found to be the result of an interaction between a few damped (oscillatory and nonoscillatory) modes with decay time scales lying in a range of 20–800 years. The amplification mechanism is also found to be distinct from the advective feedback leading to THC instabilities for large freshwater forcing.

1. Introduction

The thermohaline circulation (THC, meant here to represent the zonally averaged meridional overturning circulation; Wunsch 2002; Wunsch and Ferrari 2004) is found by modern observations to carry heat and volume transports in the North Atlantic of approximatively 1 PW and 15 Sv (1 PW $\equiv 10^{15}$ W and 1 Sv $\equiv 10^6$ $m^3\ s^{-1}$), respectively (Ganachaud and Wunsch 2000). The THC is therefore expected to play a crucial role in present-day climate. The stability and variability of the THC are thus critical issues for our understanding of the climate state and have been studied intensively in the past few decades (Marotzke et al. 1988; Stommel 1961; Weaver and Hughes 1992; Weaver et al. 1993). For example, general circulation models (GCMs) show that if the THC is weaken by about 25%, it might cross a stability threshold and enter an unstable regime (Tziperman 1997; Tziperman et al. 1994).

Proxy observations seem to indicate that climate, and probably also the THC, have been fairly stable for over 10 000 years, with a small amplitude variability. This small amplitude variability of the present-day THC suggests that its dynamics are linear, and possibly driven by stochastic atmospheric forcing (e.g., Griffies and Tziperman 1995). In such stable linear systems, small perturbations may undergo a strong transient amplification before eventually decaying, because of the interaction of multiple eigenmodes of the system (e.g., Farrell and Ioannou 1996) if the dynamical system is nonnormal (i.e., if its eigenvectors do not form an orthogonal basis). While there is no obvious way to predict if a dynamical system is nonnormal and how strongly nonnormal it is without examining the detailed properties of its operator, it may be stated that problems derived from fluid dynamics are generally nonnormal (e.g., Farrell 1988, 1989). The initial conditions leading to such transient growth are termed optimal initial conditions and are obtained by solving an eigenvalue problem based on the linear (or linearized) model equa-

Corresponding author address: Laure Zanna, Department of Earth and Planetary Sciences and Division of Engineering and Applied Sciences, Harvard University, Cambridge, MA 02138.
E-mail: zanna@fas.harvard.edu

tions. In addition, in a stochastically forced linear system, the spatial structure of the stochastic forcing leading to maximum variance of the model solution is referred to as stochastic optimals (Farrell and Ioannou 1996; Kleeman and Moore 1997). These concepts were applied to several climate variability phenomena such as atmospheric flows and cyclogenesis (Farrell 1988, 1989; Farrell and Ioannou 1996), the wind-driven ocean circulation (Moore 1999), and the El Niño–Southern Oscillation variability (Moore and Kleeman 1997a,b, 1999a; Penland and Sardeshmukh 1995).

Recently, transient amplification and stochastic optimals were investigated for the THC by Tziperman and Ioannou [2002; see also Lohmann and Schneider (1999) for a discussion on nonnormal dynamics and predictability of the Stommel's box model]. Two physical mechanisms for the transient amplification of the THC were found by examining the stable nonnormal THC dynamics using a simple meridional ocean box model. The first mechanism, with a transient amplification time scale of a couple of years, involves an interaction between the THC anomaly induced by rapidly decaying sea surface temperature anomalies and the THC anomaly induced by the slower-decaying salinity modes. The second mechanism of transient amplification involves an interaction between different slowly decaying salinity modes, and has a typical growth time scale of few decades. However while the THC was amplified by these mechanisms, the initial temperature and salinity anomalies did not undergo a transient amplification, limiting the potential role of the resulting transient amplification dynamics in THC variability.

The objective of the present study is to investigate possible physical mechanisms for the transient growth of THC anomalies, taking into account both the oceanic and the atmospheric dynamics using a coupled model with a higher meridional resolution than the box model used by Tziperman and Ioannou (2002). Our main result is a new mechanism of transient amplification of THC anomalies. The mechanism results in a dramatic amplification of initial temperature and salinity anomalies, as well as of the THC itself, which is far more significant than the one obtained in the simple box model of Tziperman and Ioannou (2002). The amplification is characterized by a time scale of about 40 years and exists because of the interaction of several damped oscillatory and nonoscillatory eigenmodes of the ocean model. The dramatic amplification of THC, temperature, and salinity anomalies by this mechanism indicates that transient amplification may play a significant role in the dynamics of THC variability.

The model used here was presented in Sayag et al. (2004), and is briefly described in section 2 with the modifications required for the present study. A summary of the model equations in their continuous form and of the relevant model parameters is given in the appendix. Following this, section 3 presents the linearized model dynamics, and section 4 discusses the optimal initial conditions leading to a transient amplification of THC anomalies. We conclude in section 5.

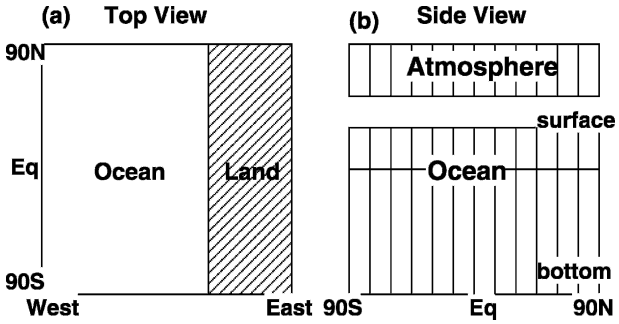

FIG. 1. (a) Top view of the model's surface (lat vs lon) shows the land and ocean areas. (b) A latitude vs depth cross section through the ocean and atmosphere models. The vertical lines schematically mark a few of the grid boxes in the atmosphere and ocean. The latitudinal resolution throughout the ocean and atmosphere is 3°.

2. Model description

The model used for the present work is a two-dimensional coupled atmosphere–ocean model averaged in the longitudinal dimension and with a relatively high resolution in the meridional direction. The model, schematically shown in Fig. 1, includes one landmass that occupies 30% of the total surface, and is basically that developed by Sayag et al. (2004) with some modifications that will be described below. The atmosphere is a one-layer vertically averaged energy balance model for the potential temperature θ and humidity q. The ocean model is composed of two vertical layers with thicknesses H_{top} and H_{bot} for the surface and the deep ocean, respectively. The finite difference meridional resolution is $\Delta y = 3°$ ($n = 61$ latitudinal cells) in all runs presented here. The ocean temperature T and salinity S are governed by advection–diffusion equations. When the vertical ocean stratification is unstable, the two levels are instantaneously mixed to vertically uniform temperature and salinity profiles. The dynamics are hydrostatic, mass conserving, and based on the Boussinesq approximation. The ocean meridional velocity $v(y)$ satisfies a balance of frictional and pressure gradient terms in the meridional momentum equation. The meridional velocity at latitude y of the upper-ocean layer is therefore calculated from the density gradients at this lati-

tude, following the usual expression used in box models (Huang et al. 1992; Stommel 1961; Tziperman et al. 1994),

$$v(y) = \kappa\{H_{\text{top}}[\rho_{\text{top}}(y+1) - \rho_{\text{top}}(y)] + H_{\text{bot}}[\rho_{\text{bot}}(y+1) - \rho_{\text{bot}}(y)]\}, \quad (1)$$

where $\kappa = g\ H_{\text{bot}}/(2r_o\rho_0\Delta yD)$, g is the gravitational acceleration, r_0 is a friction coefficient, ρ_0 is the reference density, D is the ocean depth, and the density $\rho = \rho(S, T)$ is defined by a linear equation of state. The meridional transport for the upper ocean, in Sverdrups, is thus given by

$$U(y) = v(y)\Delta x f_S(y) H_{\text{top}}, \quad (2)$$

where $f_S(y)$ is the fraction of ocean in a cell at a given latitude y and $\Delta x = 4R_0$ is the longitudinal extent of the model, where R_0 is the earth's radius. The model parameters different from those in Sayag et al. (2004) are summarized in Table A1. The physical meaning of the different parameters is described in the appendix with a brief overview of the model equations.

Consider now the differences from the original model used by Sayag et al. (2004). First, the upwind scheme used originally to represent the vertical advection in the temperature and salinity equations was replaced by a central differences scheme (see the appendix). The upwind scheme is not continuous, and this discontinuity in the finite difference equations lead to a major artifact when studying the linearized dynamics of the system at the transitions points where the vertical velocity changes sign with latitude (Thuburn and Haine 2001; Zanna 2003). The second change was to include the precipitation P as a sink in the moisture equation. In the original model [Eq. (6) in Sayag et al. 2004] the moisture was calculated after every time step, and if its value was larger than the critical value $q_{\max}$, the atmosphere flushed the humidity excess as precipitation. Instead, we have changed this to a differentiable parameterization in which the precipitation term was incorporated into the moisture equation (see the appendix).

It is important to note that the physics and the solution of the model were hardly altered by the above two modifications, while the results of the linearized model and optimal initial conditions analyzed in this work were significantly improved. Last, we ignore sea ice and land ice dynamics and assume the ocean temperature to be always above freezing.

3. Dynamics of the linearized system

Before examining the possibility of transient amplification of THC anomalies, let us first analyze the linearized dynamics of the system. The nonlinear model equations (Sayag et al. 2004; see also the appendix) for the prognostic variables θ, q, T, and S can be written in the following form:

$$\frac{d\mathbf{P}(t)}{dt} = \mathbf{F}[\mathbf{P}(t)], \quad (3)$$

where $\mathbf{F}$ denotes the nonlinear model operator and $\mathbf{P}$ is the state vector specifying the time-dependent model state for the atmospheric temperature θ and moisture q, and for the temperature T and salinity S at the top and bottom ocean levels at all grid points

$$\begin{aligned}\mathbf{P} = [&\theta(y_1), \ldots, \theta(y_n),\\ &q(y_1), \ldots, q(y_n),\\ &T(y_1, z_{\text{top}}), \ldots, T(y_n, z_{\text{top}}),\\ &T(y_1, z_{\text{bot}}), \ldots, T(y_n, z_{\text{bot}}),\\ &S(y_1, z_{\text{top}}), \ldots, S(y_n, z_{\text{top}}), \quad \text{and}\\ &S(y_1, z_{\text{bot}}), \ldots, S(y_n, z_{\text{bot}})]^{\text{T}}_{1\times 366}. \end{aligned} \quad (4)$$

To analyze the possible transient amplification of the THC, and to look for optimal initial conditions, we linearize (3) about the steady state reached by the full nonlinear model (Fig. 2). As explained in the appendix, certain parameters have been chosen in order to obtained a relatively realistic steady state reflecting the present-day climate. A north–south asymmetry is obtained in the current setting using different atmospheric emissivity coefficients for the Northern and Southern Hemispheres (Table A1). The minimum in the deep-ocean temperature at the equator is unfortunately an artifact due to the use of central differences scheme for the vertical advection term in the heat equation (see the appendix). The central differences scheme is required since a more standard upwind scheme normally used for such coarse-resolution models results in difficulties when evaluating the optimal initial conditions (see section 2 and also Thuburn and Haine 2000; Zanna 2003).

Consider a small perturbation to this steady state by writing the state vector as $\mathbf{P} = \overline{\mathbf{P}} + \mathbf{P}'(t)$, where $\overline{\mathbf{P}}$ is the steady state and $\mathbf{P}'$ is the small perturbation vector. By linearizing (3), we obtain the following linear system:

$$\frac{d\mathbf{P}'}{dt} = A\mathbf{P}', \quad (5)$$

where the perturbation vector, similarly to (4), is defined by $\mathbf{P}'^{\text{T}} = (\theta', q', T', S')_{1\times 366}$ and the matrix $\mathbf{A}_{366\times 366}$ represents the linearized model equations. Since the linearized matrix $\mathbf{A}$ is time independent, the

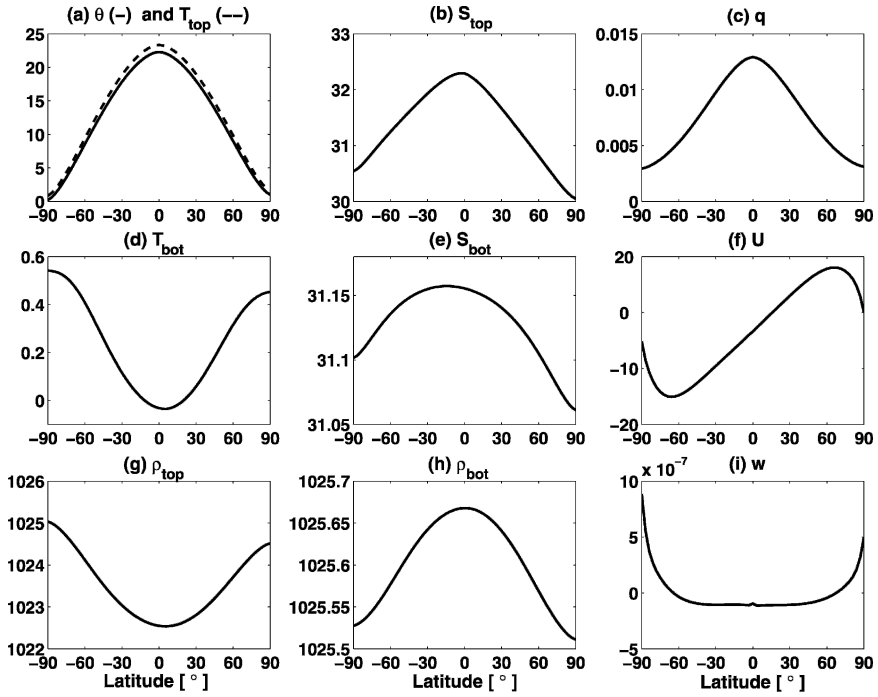

FIG. 2. The steady-state solution for the ocean and the atmosphere, reached by the full nonlinear model (a) atmospheric temperature θ (solid line) and surface ocean temperature T_{top} (dashed line) (°C), (b) surface ocean salinity S_{top} (ppt), (c) atmospheric moisture q (kg kg^{-1}), (d) deep ocean temperature T_{bot} (°C), (e) deep ocean salinity S_{bot} (ppt), (f) horizontal ocean volume transport U (Sv), (g) surface ocean density ρ_{top} (kg m^{-3}), (h) deep ocean density ρ_{bot} (kg m^{-3}), and (i) vertical ocean velocity w (m s^{-1}).

dynamical system is autonomous and its explicit solution is given by

$$\mathbf{P}'(t) = e^{\mathbf{A}t}\mathbf{P}'(t=0) = B(t,0)\mathbf{P}'(0), \tag{6}$$

where the matrix $\mathbf{B}(t,0) = e^{\mathbf{A}t} \equiv \mathbf{B}(t)$ is the propagator of the system, and $\mathbf{P}'(0) \equiv \mathbf{P}'_0$ is the perturbation state vector at $t = 0$. If all the eigenvalues of $\mathbf{A}$ are negative, then the system is stable, meaning that any small perturbation vector $\mathbf{P}'$ added to the steady state will tend to zero as $t \to \infty$. For nonnormal system, where $\mathbf{A}$ does not commute with its Hermitian transpose ($\mathbf{A}\mathbf{A}^\dagger \neq \mathbf{A}^\dagger\mathbf{A}$), the perturbation vector $\mathbf{P}'$ given by (6) may undergo a transient growth at any given finite time τ (Farrell and Ioannou 1996) before its eventual decay, as we will show below (for convenience, we will now drop the primes).

To evaluate the linearized matrix $\mathbf{A}$ of the system, the convective adjustment has been turned off. The convective adjustment parameterization is based on a switch depending on the vertical density stratification and is therefore not differentiable and may cause artifacts when linearized (see section 2). We used the optimal initial conditions calculated below using the linearized model in the fully nonlinear model, which includes the convective adjustments, and found that the amplification behavior is qualitatively not modified by nonlinearities and convection. We conclude, therefore, that the treatment of convection did not affect the relevance of our linearized analysis.

The linearized model is stable as expected, and all the eigenvalues λ of $\mathbf{A}$ are negative, meaning that any initial perturbation eventually decays. Some eigenmodes undergo a pure decay, and others are complex, and therefore oscillate and decay. The time scales for decay and oscillation are determined by the real and imaginary part of the eigenvalues respectively, such that $\tau_{\text{decay}} = |1/\text{Re}(\lambda)|$ and $\tau_{\text{oscill}} = |2\pi/\text{Im}(\lambda)|$. The decay time scales form a broad spectrum of values, from fast-decaying modes with time scale starting from O(1 h) and up to a decay time scale of O(780 yr). We find oscillatory modes with time scale varying from 20 to a few hundreds of years (Fig. 3). We note from Fig. 3 that the faster-decaying eigenmodes (where $\tau_{\text{decay}} < 2.5$ months) are not oscillating (the imaginary part of the eigenvalues is 0); the oscillatory modes are associated only with the slowest decaying modes. It was shown in previous works (Weaver and Sarachik 1991; Weaver et al. 1991) that a self-sustained interdecadal variability

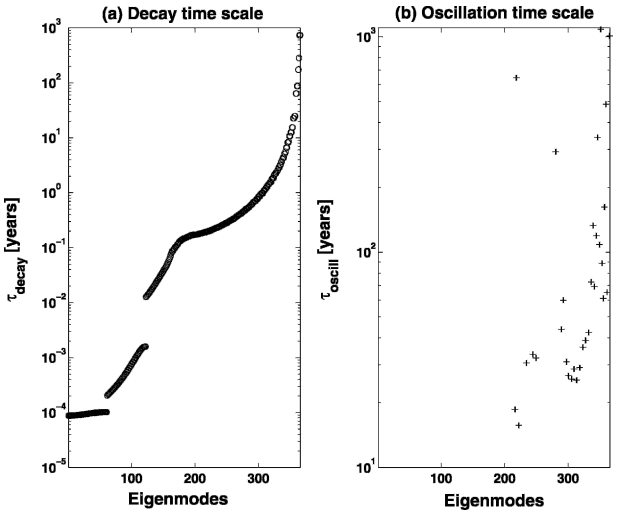

FIG. 3. (a) Decay time scale τ_{decay} and (b) oscillation time scale τ_{oscill} of the 366 eigenmodes of the linearized matrix $\mathbf{A}$ as function of the eigenmode number. (Note that the oscillatory time scale is not shown for nonoscillatory modes.)

may be obtained with a strong freshwater forcing while this variability does not exist for weaker freshwater flux. More relevant perhaps to the context of the present work, it was also shown in a linearized THC model (Griffies and Tziperman 1995; Tziperman et al. 1994) that the existence of oscillatory modes depends on the freshwater flux amplitude.

4. Optimal initial conditions and transient amplification

We wish to find mechanisms leading to transient amplification of THC anomalies in a climate regime in which the THC is stable in the sense that small perturbation decay after a sufficiently long time. To measure the growth of the state vector anomaly at time τ, $\mathbf{P}(\tau)$, defined above by (5) and (6), we need to define a norm $\|\mathbf{P}\|_{\mathbf{X}}$ involving a norm kernel $\mathbf{X}$ such that $\|\mathbf{P}(\tau)\|_{\mathbf{X}}^2 = \mathbf{P}^{\mathrm{T}}(\tau)\mathbf{X}\mathbf{P}(\tau)$. The maximization of $\mathbf{P}^{\mathrm{T}}(\tau)\mathbf{X}\mathbf{P}(\tau)$ is done while constraining the initial conditions to be of amplitude one using a possibly different norm kernel $\mathbf{Y}$, such that $\mathbf{P}_0^{\mathrm{T}}\mathbf{Y}\mathbf{P}_0 = 1$. Several norm kernels have been investigated, and some experimentation was required to find the one that results in interesting optimal initial conditions leading to an amplification of the THC anomaly. In the next sections we first (section 4a) describe some preliminary experiments with different norm kernels and explain the precise procedure for evaluating the optimal initial conditions, and then (section 4b) describe our main results, obtained using a norm kernel that produces physically interesting results. The reader is advised to proceed directly to section 4b on first reading.

a. Preliminary experiments

We start with an energy kernel under which the norm is the normalized sum of squares of all model variables. The norm kernel $\mathbf{X}$ in this case is a diagonal matrix that normalizes the variables based on their units and typical relative variability amplitudes, such that

$$\mathrm{diag}(\mathbf{X}) = \left[\left(\frac{1}{\delta\theta}\right)^2_{1\times 61}, \left(\frac{1}{\delta q}\right)^2_{1\times 61}, \left(\frac{1}{\delta T_{\text{top}}}\right)^2_{1\times 61}, \left(\frac{1}{\delta T_{\text{bot}}}\right)^2_{1\times 61}, \left(\frac{1}{\delta S_{\text{top}}}\right)^2_{1\times 61}, \left(\frac{1}{\delta S_{\text{bot}}}\right)^2_{1\times 61} \right],$$

where $\delta\theta = 5 \times 10^{-4}$°C, $\delta q = 5 \times 10^{-7}$ kg kg^{-1}, $\delta T_{\text{top}} = 5 \times 10^{-4}$°C, $\delta T_{\text{bot}} = 5 \times 10^{-5}$°C, $\delta S_{\text{top}} = 8 \times 10^{-4}$ ppt, and $\delta S_{\text{bot}} = 8 \times 10^{-5}$ ppt. In this experiment, when looking for a growth of the dimensionless quantity $\|\mathbf{P}(\tau)\|_{\mathbf{X}}^2 = \mathbf{P}^{\mathrm{T}}(\tau)\mathbf{X}\mathbf{P}(\tau)$ at different times τ, we find optimal initial conditions $\mathbf{P}(t = 0)$ and a corresponding physical mechanism that allows a growth of $\|\mathbf{P}(\tau)\|_{\mathbf{X}}^2$ with a typical time scale $O(1\ \text{yr})$ (the procedure for calculating the optimal initial conditions is given in detail below). The initial conditions correspond mostly to upper-ocean salinity anomalies, with weaker anomalies for the other model variables and maximize the growth of temperature, salinity, and all other variables but not of the overturning circulation itself. The physical mechanism behind this growth is the following: the initial salinity anomalies in the upper-ocean layer create a perturbation velocity v', driven mostly by salinity anomalies. The velocity perturbation then advects the background temperature and salinity, enhancing the anomaly vector with a dominant growth in the upper-ocean temperature.

Given that our interest here is in THC growth, we proceed to use a kernel that maximizes the growth of the THC, rather than the normalized sum of squares of the prognostic model variables. The model THC at a given latitude y and time τ depends linearly on the density gradients at that latitude, and Eq. (2) for the THC anomaly may therefore be written as $U(y, t = \tau) = \mathbf{R}_j^{\mathrm{T}}\mathbf{P}(t = \tau)$, where

$$\mathbf{R}_j = [\mathbf{R}_j^{\text{atm}}, \mathbf{R}_j^{\mathrm{T}}, \mathbf{R}_j^{S}]^{\mathrm{T}}, \tag{7}$$

where

$$\begin{aligned}
\mathbf{R}_j^{\text{atm}} &= (0_{1\times 122})^{\mathrm{T}},\\
\mathbf{R}_j^{\mathrm{T}} &= [0_{1\times(j-1)}, \tilde{\kappa}\alpha H_{\text{top}}, -\tilde{\kappa}\alpha H_{\text{top}}, 0_{1\times(60-j)}, 0_{1\times(j-1)},\\
&\qquad -\tilde{\kappa}\alpha H_{\text{bot}}, \tilde{\kappa}\alpha H_{\text{bot}}, 0_{1\times(60-j)}]^{\mathrm{T}}, \quad \text{and}\\
\mathbf{R}_j^{S} &= [0_{1\times(j-1)}, -\tilde{\kappa}\beta H_{\text{top}}, \tilde{\kappa}\beta H_{\text{top}}, 0_{1\times(60-j)}, 0_{1\times(j-1)},\\
&\qquad \tilde{\kappa}\beta H_{\text{bot}}, -\tilde{\kappa}\beta H_{\text{bot}}, 0_{1\times(60-j)}]^{\mathrm{T}}.
\end{aligned} \tag{8}$$

The latitude index j satisfies $y = -90 + \Delta y(j - 1)$ with $j = 1, 2, \ldots, n$; the parameter $\tilde{\kappa}$ is given by $\tilde{\kappa} = \kappa \Delta x f_s(y) H_{\text{top}}$, where κ, Δx, $f_s(y)$, and H_{top} were defined in section 2, $0^{\text{T}}_{1\times q}$ is a zero vector of dimension q, and $\alpha = 0.1713$ kg m^{-3} K^{-1} and $\beta = 0.781$ kg m^{-3} are the thermal and salinity expansion coefficients, respectively. Since the model is of a relatively high resolution in the y direction (as compared with simple box model), the calculation of optimal initial conditions using a norm kernel that maximizes the transient growth of the THC at a given latitude turns out to be dynamically uninteresting. The optimal initial conditions found by maximizing the THC anomaly at a given latitude y have a vanishing THC anomaly at this latitude, and very high THC anomalies at adjacent grid points. At following times, the THC at latitude y increases as the neighboring THC anomalies move toward y and decrease at other latitudes. Hence, more interesting results may be obtained by maximizing the sum of squares of the THC anomaly over the entire ocean domain, between the latitudes 90°S and 90°N.

To find the optimal initial conditions that maximize the sum of squares of the THC anomaly amplitude over the entire domain, at a time τ, we define the quantity to be maximized as

$$\mathcal{J}(t = \tau) = \sum_{y=90S}^{y=90N} |U(y, t = \tau)|^2$$

$$= \sum_{j=1}^{n} [\mathbf{P}(t = \tau)^{\text{T}} \mathbf{R}_j \mathbf{R}_j^{\text{T}} \mathbf{P}(t = \tau)]. \quad (9)$$

Since $\mathbf{P}(t = \tau) = \mathbf{B}(\tau)\mathbf{P}_0$ is independent of y, the sum of squares of the THC amplitude is

$$\mathcal{J}(t = \tau) = \mathbf{P}_0^{\text{T}} \mathbf{B}(\tau)^{\text{T}} \left[\sum_{j=1}^{n} (\mathbf{R}_j \mathbf{R}_j^{\text{T}}) \right] \mathbf{B}(\tau)\mathbf{P}_0$$

or

$$\mathcal{J}(t = \tau) = \mathbf{P}_0^{\text{T}} \mathbf{B}(\tau)^{\text{T}} \mathbf{X} \mathbf{B}(\tau)\mathbf{P}_0, \quad (10)$$

where the norm matrix $\mathbf{X}$ is

$$\mathbf{X} = \sum_{j=1}^{n} (\mathbf{R}_j \mathbf{R}_j^{\text{T}}). \quad (11)$$

The norm kernel $\mathbf{X}$ given by (11) is singular (i.e., its determinant is zero) and may result in an infinite amplification and nonuniqueness of the optimal modes. It is therefore necessary to regularize the norm kernel $\mathbf{X}$ as described in more details in Tziperman and Ioannou (2002). We maximize $\mathcal{J}(t = \tau)$ subject to the constraint that $\mathbf{P}_0$ has a unit norm under some possibly different norm kernel $\mathbf{Y}$, such that $\|\mathbf{P}_0\|^2_{\mathbf{Y}} = \mathbf{P}_0^{\text{T}} \mathbf{Y} \mathbf{P}_0 = 1$.

This constrained optimization problem is solved using the Lagrange multipliers denoted here by γ (Farrell 1988):

$$\max_{\mathbf{P}_0} \{\mathbf{P}_0^{\text{T}} \mathbf{B}(\tau)^{\text{T}} \mathbf{X} \mathbf{B}(\tau, 0)\mathbf{P}_0 + \gamma[\mathbf{P}_0^{\text{T}} \mathbf{Y} \mathbf{P}_0 - 1]\}, \quad (12)$$

and the maximum occurs where

$$\frac{\partial}{\partial \mathbf{P}_0} \{\mathbf{P}_0^{\text{T}} \mathbf{B}(\tau)^{\text{T}} \mathbf{X} \mathbf{B}(\tau)\mathbf{P}_0 + \gamma[\mathbf{P}_0^{\text{T}} \mathbf{Y} \mathbf{P}_0 - 1]\} = 0. \quad (13)$$

The initial conditions $\mathbf{P}_0$ leading to an optimal growth of $\mathcal{J}$ at a time $t = \tau$ are therefore the generalized eigenvectors of the generalized eigenproblem,

$$\mathbf{B}(\tau)^{\text{T}} \mathbf{X} \mathbf{B}(\tau)\mathbf{P}_0 = -\gamma \mathbf{Y} \mathbf{P}_0, \quad (14)$$

where the generalized eigenvalue γ reflects the amplification of $\mathcal{J}(t = \tau)$ if the two kernels $\mathbf{X}$ and $\mathbf{Y}$ are equal.

We first calculated the optimal initial conditions that maximize the sum of squares of the THC (10) subject to $\|\mathbf{P}_0\|^2_{\mathbf{Y}} = \mathbf{P}_0^{\text{T}} \mathbf{Y} \mathbf{P}_0 = 1$, where $\mathbf{Y} = \mathbf{X}$ is the norm kernel defined by (11), reflecting the sum of squares of the THC amplitude over the entire ocean domain. Using this kernel, we found a physical mechanism, which appears to again be physically irrelevant, that allows for transient amplification of the THC anomaly with a fast time scale of O(1 day), regardless of the optimization time τ. The optimal initial conditions involve mostly a positive moisture anomaly in the atmosphere, between the latitudes 78° and 90°S, which increases the initial precipitation over those latitudes, while a negative moisture anomaly between 78° and 60°S decreases it in that region. The model time evolution starting from these initial conditions creates large salinity anomalies and therefore large gradients of density anomalies, and amplifies the THC in the Southern Ocean. Although the temperature of the ocean is affected by the initial conditions, the THC anomaly is mainly driven by salinity gradients.

This mechanism is clearly not of interest as it is based on physically unrealizable large moisture anomalies, and produces a too rapid response, regardless of the optimization times τ. To eliminate the possibility of such dominant moisture anomalies in the optimal initial conditions, we proceed to define a new norm kernel $\mathbf{Y}$, which is used to constrain the initial conditions in (12). This allows us to obtain more relevant time scales and mechanism for a THC amplification involving initial ocean temperature and salinity anomalies rather than nonphysically realizable moisture anomalies.

We therefore require that the initial conditions satisfy $\|\mathbf{P}_0\|^2_{\mathbf{Y}} = \mathbf{P}_0^{\text{T}} \mathbf{Y} \mathbf{P}_0 = 1$, where $\mathbf{Y} = \mathbf{X} + \mathbf{F}$. The matrix $\mathbf{F}_{366\times366}$ is a diagonal matrix such that its entire diagonal is zero except the elements $\mathbf{F}_{62\to122,62\to122}$ corresponding to the atmospheric moisture, which are set to

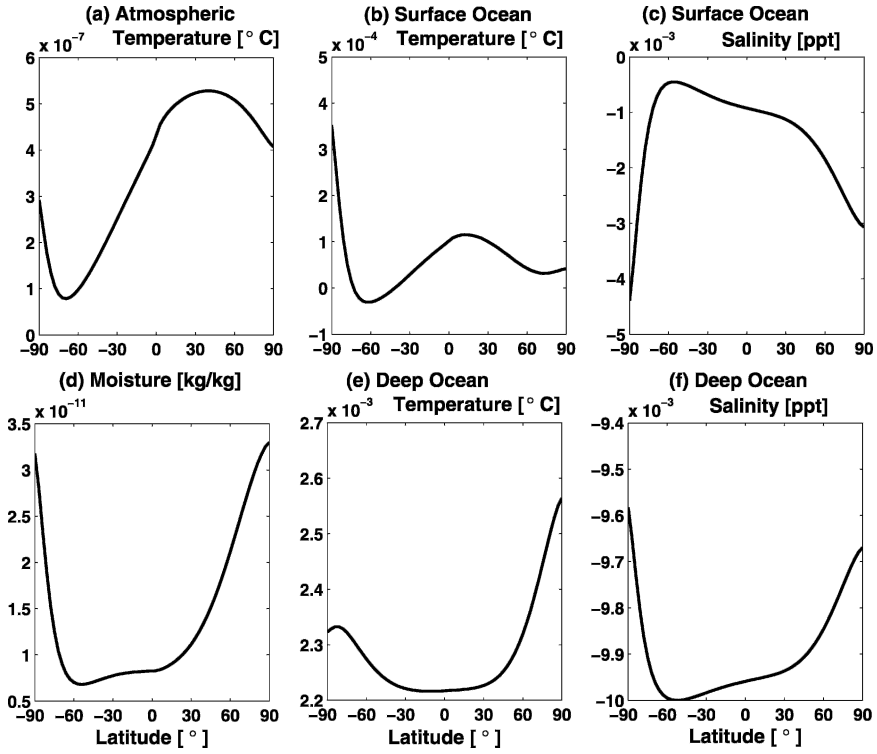

FIG. 4. Optimal initial conditions as function of latitude, found using the linearized model, leading to the amplification of the THC after 42 yr. (a) Atmospheric temperature anomalies θ, (b) moisture anomalies q, (c) surface temperature anomalies T_{top}, (d) deep temperature anomalies T_{bot}, (e) surface salinity anomalies S_{top}, and (f) deep salinity anomalies S_{bot}.

10^4. This somewhat arbitrary value corresponds to the smallest value of $\mathbf{F}_{62\to122,62\to122}$ resulting in a fairly complete elimination of the initial atmospheric moisture anomalies in the optimal initial conditions. The norm of the initial conditions $\mathbf{P}_0$, under the defined kernel $\mathbf{Y}$, should be equal to 1 and is defined by

$$\|\mathbf{P}_0\|^2_{\mathbf{Y}} = \mathbf{P}_0^{\mathrm{T}}\mathbf{X}\mathbf{P}_0 + \sum_{i=1}^{366} F_{ii}P_{0,i}^2 = 1.$$

Thus, because of the large kernel values $\mathbf{F}_{ii}$ corresponding to the moisture anomaly and in order to satisfy the constraint on the norm vector, the optimal initial values for the atmospheric moisture must take very small values. In summary, the matrix $\mathbf{F}$ was added to the kernel in order to force a very small initial moisture anomaly.

We proceed to use this kernel to search for initial conditions resulting in an optimal transient amplification of the THC for different optimization times τ.

b. Optimal amplification of THC anomalies

The above preliminary experiments led us to the use of the above norm kernels $\mathbf{X}$ and $\mathbf{Y}$, which maximize the sum of squares, over the entire domain, of the THC anomaly amplitude. These kernels also suppress physically nonrealizable large atmospheric moisture anomalies in the optimal initial conditions as explained above. An interesting physical mechanism was found using these kernels, with a typical time scale of 42 yr, and involving mostly oceanic temperature and salinity anomalies (Fig. 4). The initial THC vanishes because of a cancellation between the initial temperature and salinity anomalies, so that the actual amplification of the initial THC anomaly is formally infinite (Tziperman and Ioannou 2002).

More significantly, the optimal initial conditions found using the linearized model for $\tau = 42$ yr induce a rapid growth of basically most of the model variables, as seen in Fig. 5. The figure shows the time-versus-latitude plots of the oceanic and atmospheric variables. Only a few contour lines, if any, cross the $t = 0$ axis in the different panels of this figure, indicating that the amplitude of the variables at $t = 0$ is very small relative to their maximal amplitude obtained after about 40 years. The THC, in particular, starts exactly at zero, and is significantly amplified. More interesting is that the temperature and salinity are also amplified quite dramatically, as will be discussed shortly.

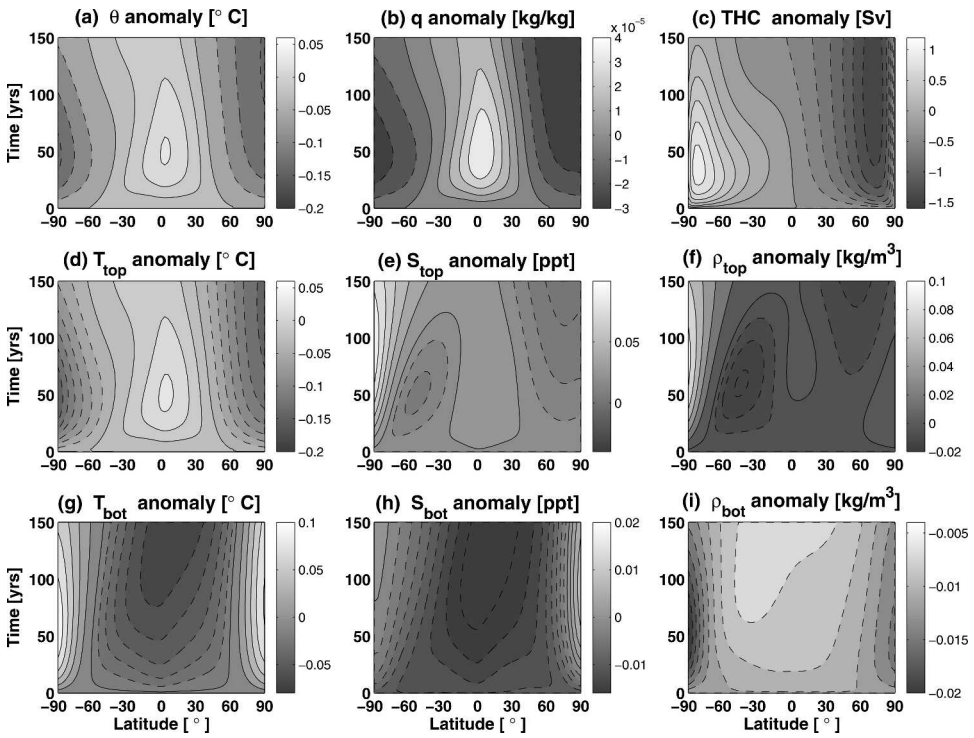

FIG. 5. The linearized model evolution starting from the optimal initial conditions resulting in a maximum amplification of the THC after 42 yr. Different model variables are shown as function of latitude and time: (a) atmospheric temperature anomalies, (b) moisture anomalies, (c) THC anomaly, (d) surface temperature anomalies, (e) surface salinity anomalies, (f) surface density anomalies, (g) deep temperature anomalies, (h) deep salinity anomalies, and (i) deep density anomalies.

Initially, a rapid amplification of the bottom temperature anomalies (Fig. 5g) of the ocean causes the amplification of the THC seen in Fig. 5c, for $\tau = 42$ yr. During the first few months, the THC anomaly is mostly driven by surface salinity anomalies (Fig. 6c). After a few months, a bottom temperature anomaly develops because of advection of the mean temperature field by the THC anomaly. This rapidly increasing bottom temperature anomaly also contributes to the THC anomaly, and eventually overcomes the contribution from the surface salinity. The THC amplification is slower now (Fig. 6b). Once the peak of the amplification occurs, the anomalies decay with a slow time scale of hundreds of years. The slow decay of the ocean anomalies is due to horizontal and vertical diffusion of salinity and temperature after they have been redistributed over the ocean via advection by the mean flow. A significant part of the temperature anomalies is also transferred to the atmosphere by air–sea interaction and is dissipated there by long wave radiation.

The mechanism of transient amplification may be briefly described as follows Farrell and Ioannou (1996). The initial conditions are a combination of several eigenmodes of the linearized operator **A**. These eigenmodes are characterized by different decaying time scales where some of these modes decay rapidly, while others decay more slowly. The contributions from these eigenmodes to the initial conditions are large and nearly cancel each other at $t = 0$, resulting in an initial condition of relatively small amplitude. This mutual cancellation is possible due the nonorthogonality of the eigenmodes since the operator **A** is nonnormal. At later time, the rapid decay of the fast eigenmodes, which eliminates the initial cancellation, leaves the solution nearly equal to the large amplitude of the slow-decaying modes, causing the initial amplification. The solution then eventually decays along with the slow-decaying eigenmodes.

Given this mechanism of transient amplification, it is thus insightful to investigate the eigenmodes of the linearized matrix **A**, which participate in the transient growth. These modes were found by projecting the initial conditions $\mathbf{P}_0$ on the eigenmodes of the linearized system (Farrell and Ioannou 1996). Let us denote by $\{\lambda_i, \mathbf{s}_i\}$ and $\{\sigma_i, \mathbf{r}_i\}$ the set of {eigenvalues, eigenvectors} of the linearized matrix **A** and of its Hermitian transpose $\mathbf{A}^\dagger$, respectively. The initial state vector $\mathbf{P}_0$ can be

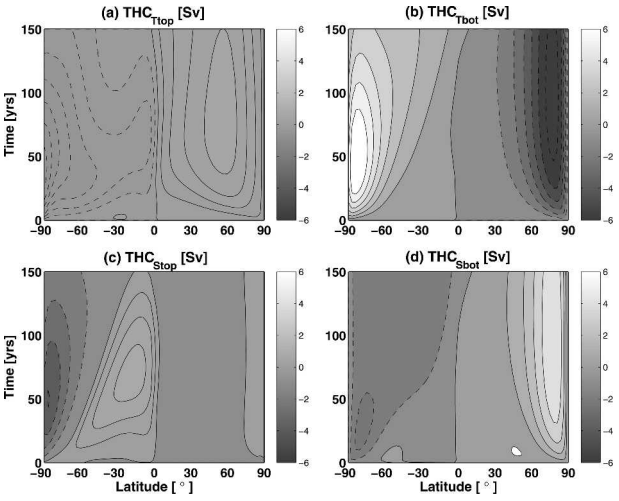

FIG. 6. The different THC components due to the contribution of the (a) surface temperature anomalies, (b) deep temperature anomalies, (c) surface salinity anomalies, and (d) deep salinity anomalies, as function of time and latitude.

written as a linear superposition of the eigenmodes of **A**, such that

$$\mathbf{P}_0 = \sum_{k=1}^{k=366} a_k \mathbf{s}_k. \tag{15}$$

To find the coefficients a_k, which are the projections of $\mathbf{P}_0$ on the eigenmodes $\mathbf{s}_i$, we multiply (15) by $\mathbf{r}_k^{\mathrm{T}}$.

The biorthogonality property of the eigenmodes of the linearized matrix **A** and of its Hermitian transpose $\mathbf{A}^{\dagger}$, states that

$$\mathbf{s}_i^{\mathrm{T}} \mathbf{r}_j (\sigma_i - \lambda_j^*) = 0. \tag{16}$$

The eigenvalues of **A** and its Hermitian transpose $\mathbf{A}^{\dagger}$ are ordered such that for $i = j$ we have $\sigma_i = \lambda_j^*$. Therefore for $i \neq j$, and assuming that $\lambda_i \neq \lambda_j$, we obtain that $\mathbf{s}_i^{\mathrm{T}} \mathbf{r}_j = 0$ as a result of (16). Using this result we find that the projection of the initial conditions on the eigenmodes is given by $a_k = (\mathbf{r}_k^{\mathrm{T}} \mathbf{P}_0)/(\mathbf{r}_k^{\mathrm{T}} \mathbf{s}_k)$.

The largest of the coefficients a_k corresponds to the main eigenmodes contributing to the optimal initial conditions and participating in the transient amplification. We find that the transient amplification of the THC is mainly due to the interaction of five slow-decaying modes: four oscillatory eigenmodes and their complex conjugates and one nonoscillatory eigenmodes. The decay times of these modes are 23, 25, 87, 281, and 784 yr, and their oscillation periods are 61, 162, 65, 0, and 1000 yr, respectively.

The optimal initial conditions are mostly composed of a surface salinity anomaly, and surface and deep temperature anomalies. Figure 7a shows the initial structure of the ocean temperature and salinity corresponding to each of these five dominant modes, calculated from the elements of the vector

$$\mathbf{P}_{0_l} = a_l \mathbf{s}_l + c.c., \tag{17}$$

where c.c. denotes complex conjugate. In addition, Fig. 7b also shows the contribution of each of these modes to the THC anomaly, $U_l(y, t)$, calculated from the projection of the optimal initial temperature and salinity on the THC (Fig. 7b),

$$U_l(y, t) = \mathbf{R}_j^{\mathrm{T}} \mathbf{B}(t) a_l \mathbf{s}_l + c.c., \tag{18}$$

where $l = 1, 2, 3, 4, 5$ (for each of the dominant eigenmodes participating in the transient growth) and $\mathbf{R}_j$ is given by (7) and (8). The relatively rapid decay of the first two oscillatory eigenmodes, with decay time scales of 23 and 25 yr, leaves only the least damped modes ($\tau_{\mathrm{decay}} = 87$, 281, and 784 yr) of the system after few decades, explaining the 40-yr time scale of the transient growth in Fig. 5. The sum of these five eigenmodes reproduces the amplification of the THC anomaly fairly well, although when reconstructed from only these five modes, the initial THC is not exactly zero. In fact, while these five modes are sufficient to explain the amplification of the THC, in order to produce the dramatic growth observed above (Fig. 5) in the temperature and salinity, a combination of many more of the 366 eigenmodes of our linearized model equations is necessary [equivalently, additional terms are needed in (15) to explain the results in Fig. 5].

To further understand the physical mechanism of transient THC growth, we have performed many experiments, using both the linearized and fully nonlinear models, selectively eliminating different terms from the temperature and salinity equations. We find that eliminating the advection of the mean gradient of both the temperature and salinity by the anomalous THC (i.e., eliminating both $v'\nabla\overline{T}$ and $v'\nabla\overline{S}$) results in the elimination of the initial THC amplification (Fig. 8b). Eliminating the advection of the anomaly gradients by the mean flow ($\overline{v}\nabla T'$ and $\overline{v}\nabla S'$) mostly makes the eventual decay of the anomalies much slower (Fig. 8a). We conclude that the advection by the anomalous velocity is responsible for the transient amplification, while the advection by the mean velocity is responsible for the eventual decay. Unlike the case for the advective instability mechanism of the THC (Marotzke et al. 1988; Tziperman et al. 1994), where the advection of the mean salinity is responsible for the instability, here both temperature and salinity seem to play an equally dominant role in the transient growth of the THC anomalies.

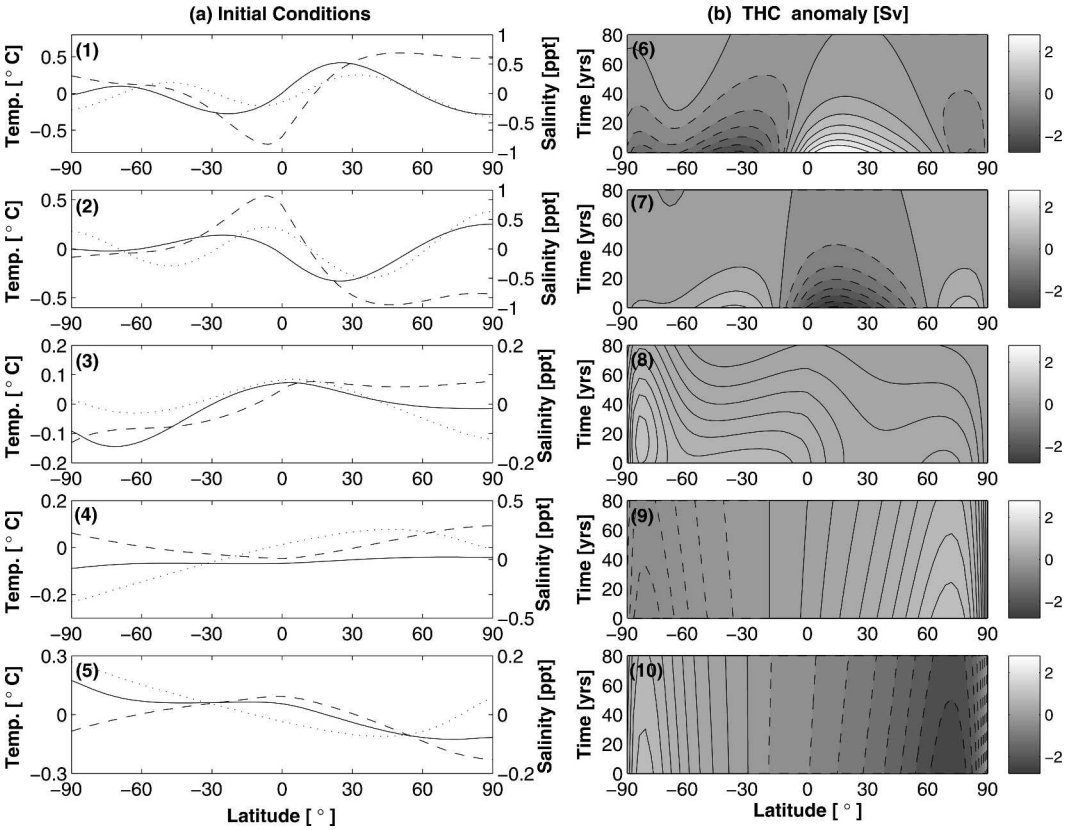

FIG. 7. Main eigenmodes participating in the transient amplification: (a) the initial conditions $\mathbf{P}_{0_k}$ for the five dominant eigenmodes contributing to the transient growth of the THC anomalies. The solid line represents the surface salinity anomaly, the dotted line represents the deep temperature anomaly and the dashed line represents the surface temperature anomaly. 1) Initial conditions associated with the first eigenmode ($\tau_{\text{decay}} = 23$ yr), 2) initial conditions associated with the second eigenmode ($\tau_{\text{decay}} = 25$ yr), 3) initial conditions associated with the third eigenmode ($\tau_{\text{decay}} = 87$ yr), 4) initial conditions associated with the fourth eigenmode ($\tau_{\text{decay}} = 281$ yr), 5) initial conditions associated with the least damped eigenmode ($\tau_{\text{decay}} = 784$ yr); (b) 6–10 time evolution of the THC anomalies resulting from the initial anomalies 1–5.

It is important to note that the transient amplification found here is significantly more interesting than the one found in a simple box model by Tziperman and Ioannou (2002). In their study, the THC also vanishes initially because of a cancellation of the temperature and salinity effects. Then, the temperature anomalies rapidly decay because of atmospheric dissipation, and the THC grows to the amplitude dictated by the initial salinity anomalies. Finally, the salinity anomalies slowly decay, and the THC with them. No significant amplification of the initial temperature and salinity anomalies was found in the mechanism found by Tziperman and Ioannou (2002), so that the maximal THC amplitude is completely controlled by the amplitude of the initial salinity anomalies.

Things are far more dramatic here. The root-mean-square of the initial temperature and salinity anomalies grow by a factor of 650 and 20, respectively, and the temperature and salinity maxima by a factor 400 and 18, respectively, within the 42 years of the transient amplification (Fig. 5). The THC grows not only because of the damping of temperature anomalies by the atmosphere, but simply because of the initial growth of the temperature and salinity. This means that, unlike in the box model study of Tziperman and Ioannou (2002), small initial temperature and salinity anomalies may result in a large eventual THC anomaly. If such optimal initial conditions can be excited by atmospheric forcing, then the resulting growth may clearly play an important role in THC and climate variability.

5. Conclusions

We used a zonally averaged coupled ocean–atmosphere model with a 3° resolution in the meridional direction in order to examine optimal initial con-

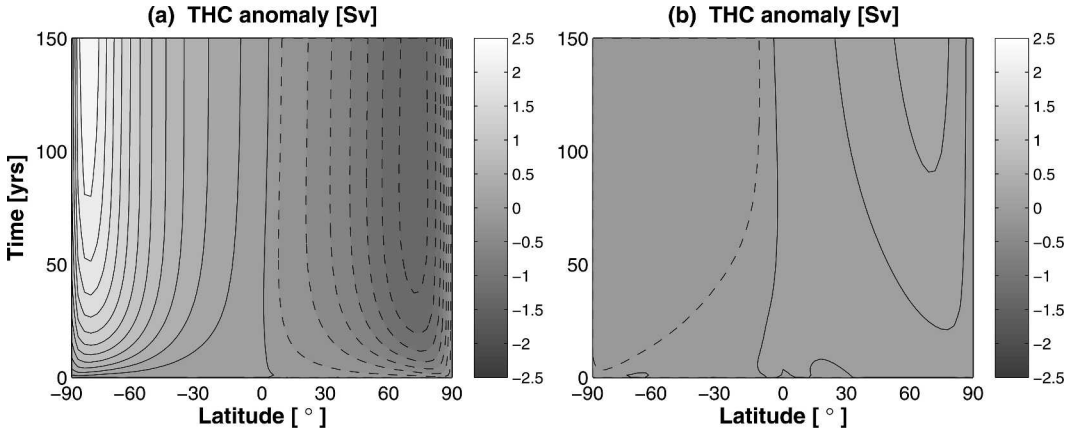

FIG. 8. The mechanism of transient growth: evolution of the THC anomaly as function of latitude and time in (a) a model experiment where $\bar{v}\nabla T'$ and $\bar{v}\nabla S'$ are eliminated, and (b) in an experiment where $v'\nabla\bar{T}$ and $v'\nabla\bar{S}$ are eliminated. These results demonstrate that the advection by the anomaly circulation causes the amplification, and the advection by the mean flow causes the eventual decay.

ditions leading to a transient growth of THC anomalies. We identified a new and interesting physical mechanism that leads to a significant transient amplification of temperature and salinity anomalies, in addition to the THC itself.

The characteristic time scale for the transient growth is about 40 years, followed by a decay of the anomalies on a centennial time scale. This mechanism is activated by the interaction of mainly five slow-decaying eigenmodes with decay time scales between 20 and 800 years. The initial THC anomaly vanished in this mechanism, as in Tziperman and Ioannou (2002), because of the exact cancellation of the THC anomalies driven by the initial temperature anomalies and those driven by the initial salinity anomalies.

The transient amplification mechanism found here for the THC is far more interesting and dramatic than the corresponding one found in a simple box model of Tziperman and Ioannou (2002). In that study, the THC grows because of the damping of initial temperature anomalies by the atmosphere, and after that initial damping, the THC is controlled by the amplitude of the initial salinity anomalies. There is no growth of the initial temperature and salinity anomalies in that model. In our study, however, the initial temperature and salinity anomalies grow significantly, by factors of about 400 and 20, respectively, during the first 40 years. Thus, unlike in the box model study of Tziperman and Ioannou (2002), *small* initial temperature and salinity anomalies may result in *large* temperature, salinity, and THC anomalies at the time of maximum amplification. In addition, this amplification mechanism is due to the advection of both mean temperature and salinity by the perturbed velocity and not only by advection of mean salinity as in the classical advective THC instability mechanism (Marotzke et al. 1988; Tziperman et al. 1994).

While the analysis presented here finds interesting optimal initial conditions and a corresponding transient amplification mechanism of the THC, we should point out that these optimal initial conditions depend on the dynamics and model configuration. In addition, we did not address the question of how such optimal initial perturbations can be realized. This will require the calculation of such optimal initial conditions (and stochastic optimals, Farrell and Ioannou 1996; Moore and Kleeman 1999b) in a 3D ocean model. The structure of these optimal modes will then need to be compared with the analysis of atmospheric variability, in order to see if the observed atmospheric variability may project on the optimal initial conditions. The use of a 3D rather than a zonally averaged model will be essential for a meaningful comparison between the horizontal structure of the optimal modes and of the atmospheric variability. We feel that the results of the present study justify further pursuing this research direction with such more realistic ocean models.

Acknowledgments. We are grateful to two anonymous referees for their constructive and useful comments. This work was supported by the James S. McDonnell foundation. We thank Roiy Sayag for providing his model code and advice for this work.

APPENDIX

Model Equations

In this appendix, we present the model equations in their continuous form and explain the parameters used

in Table A1. The potential temperature θ at latitude y is calculated from a balance between incoming solar shortwave radiation (SWR), outgoing longwave radiation (LWR), and heat exchange with the ocean and meridional heat transport (Marotzke and Stone 1995; Rivin and Tziperman 1997),

$$\frac{\partial\theta(y)}{\partial t} = \frac{2^{R_d/C_p^{\text{air}}} g}{P_0 C_p^{\text{air}}}\left[H_{\text{land}}^{\text{SW}}(y) - H^{\text{LW}}(y) - H_{\text{air-sea}}(y) + \frac{\partial}{\partial y}F_{\text{merid}}(y)\right], \quad \text{(A1)}$$

where C_p^{air} is the atmospheric specific heat capacity, and R_d the gas constant for dry air. The atmospheric emissivity $\varepsilon(y)$ appears in the expression for the outgoing longwave radiation and is represented by a parabolic profile [unnumbered equation under Eq. (4) in Sayag et al. 2004]. The parameters ε_0, ε_N, and ε_S in Table A1 are the equatorial, North Pole, and South Pole emissivities, respectively. The restoring time scale, τ, appears in the equation for the air–sea interaction [Eq. (3) in Sayag et al. 2004]. The coefficients C_1 and C_2 appear in the parametrization of the meridional heat flux [Eq. (5) in Sayag et al. 2004]. These coefficients were chosen such that the maximal value of the meridional heat flux in the Northern Hemisphere is approximatively 5 PW, close the present-day value (Trenberth and Caron 2001).

The equation governing the atmospheric humidity balances sources and sinks due to evaporation from the ocean $E(y)$, precipitation $P(y)$, and meridional moisture transport convergence $(\partial/\partial y)F_{Mq}(y)$, and is given by (Peixoto and Oort 1992)

$$\frac{\partial q(y)}{\partial t} = \frac{g\rho_w}{P_o}\left[E(y) - P(y)\frac{\Delta t}{\tau_p} + \frac{1}{\Delta x}\frac{\partial}{\partial y}F_{Mq}(y)\right]. \quad \text{(A2)}$$

The drag coefficient, C_w, appears in the parameterization of the evaporation [Eq. (7) in Sayag et al. 2004] and is chosen such that the average of evaporation minus precipitation over the latitudes 45°–90°N is about -0.2 m yr^{-1} (Peixoto and Oort 1992). The parameters K_1 and K_2 appear in the parameterization of the meridional moisture transport and are chosen such that the maximal meridional moisture in the Northern Hemisphere is about 0.38 Sv (Schmitt 1994).

The ocean temperature is governed by a simple advection–diffusion equation, which for the upper layer takes the form

$$\frac{\partial T_{\text{top}}}{\partial t} + \frac{\partial(\upsilon T_{\text{top}})}{\partial y} + \frac{w}{H_{\text{top}}}\hat{T} = K_y^{\text{T}}\frac{\partial^2 T_{\text{top}}}{\partial y^2} + \frac{1}{H_{\text{top}}}\left[2K_z^{\text{T}}\frac{T_{\text{top}} - T_{\text{bot}}}{D} + \frac{H_{\text{surf}}^{\text{T}}(y)}{\rho_0 C_P^{\text{water}}}\right], \quad \text{(A3)}$$

TABLE A1. Model parameters that are different from those used by Sayag et al. (2004).

Parameter	Value	Units
ε_0, ε_{N}, ε_{S}	0.42, 0.70, 0.71	—
C_w	1×10^{-3}	—
K_1	3.22×10^{14}	m^4 s^{-1}
K_2	1.28×10^{19}	m^5 s^{-1} K^{-1}
C_1	2.5×10^{19}	J s^{-1} K^{-1}
C_2	1.25×10^{26}	J m s^{-1} K^{-2}
τ, τ_p	100, 0.9	days, h
r_0	2×10^{-4}	s^{-1}
D	5500	m
K_y^T, K_y^S	5×10^3	m^2 s^{-1}
K_z^T, K_z^S	2×10^{-4}	m^2 s^{-1}

where C_p^{water} is the ocean water specific heat capacity; K_y^T and K_z^T are the meridional and vertical diffusion coefficients, respectively; and $\hat{T} = (T_{\text{top}}H_{\text{top}} + T_{\text{bot}}H_{\text{bot}})D^{-1}$.

The salinity S varies because of evaporation and precipitation [together, $H_{\text{surf}}^S(y)$] as well as advection and diffusion in the ocean. The salinity equation for the upper layer of the ocean is

$$\frac{\partial S_{\text{top}}}{\partial t} + \frac{\partial(\upsilon S_{\text{top}})}{\partial y} + \frac{w}{H_{\text{top}}}\hat{S} = K_y^S\frac{\partial^2 S_{\text{top}}}{\partial y^2} + \frac{2K_z^S}{H_{\text{top}}}\frac{S_{\text{top}} - S_{\text{bot}}}{D} + H_{\text{surf}}^S(y), \quad \text{(A4)}$$

where K_y^S and K_z^S are the meridional and vertical salinity diffusion coefficients, respectively; and $\hat{S} = D^{-1}(S_{\text{top}}H_{\text{top}} + S_{\text{bot}}H_{\text{bot}})$.

REFERENCES

Farrell, B. F., 1988: Optimal excitation of neutral Rossby waves. *J. Atmos. Sci.,* **45,** 163–172.

——, 1989: Optimal excitation of baroclinic waves. *J. Atmos. Sci.,* **46,** 1193–1206.

——, and P. J. Ioannou, 1996: Generalized stability theory. Part I: Autonomous operators. *J. Atmos. Sci.,* **53,** 2025–2040.

Ganachaud, A., and C. Wunsch, 2000: Improved estimates of global ocean circulation, heat transport and mixing from hydrographic data. *Nature,* **408,** 453–457.

Griffies, S. M., and E. Tziperman, 1995: A linear thermohaline oscillator driven by stochastic atmospheric forcing. *J. Climate,* **8,** 2440–2453.

Huang, R. H., J. R. Luyten, and H. M. Stommel, 1992: Multiple equilibrium states in combined thermal and saline circulation. *J. Phys. Oceanogr.,* **22,** 231–246.

Kleeman, R., and A. M. Moore, 1997: A theory for the limitation of ENSO predictability due to stochastic atmospheric transients. *J. Atmos. Sci.,* **54,** 753–767.

Lohmann, G., and J. Schneider, 1999: Dynamics and predictability of Stommel's box model: A phase-space perspective with implications for decadal climate variability. *Tellus*, **51A,** 326–336.

Marotzke, J., and P. H. Stone, 1995: Atmospheric transports, the thermohaline circulation, and flux adjustments in a simple coupled model. *J. Phys. Oceanogr.,* **25,** 1350–1364.

——, P. Welander, and J. Willebrand, 1988: Instability and multiple steady states in a meridional-plane model of the thermohaline circulation. *Tellus,* **40A,** 162–172.

Moore, A. M., 1999: Wind-induced variability of ocean gyres. *Dyn. Atmos. Oceans,* **29,** 335–364.

——, and R. Kleeman, 1997a: The singular vectors of a coupled ocean-atmosphere model of ENSO, I, thermodynamics, energetics and error growth. *Quart. J. Roy. Meteor. Soc.,* **123,** 953–981.

——, and ——, 1997b: The singular vectors of a coupled ocean-atmosphere model of ENSO, II, sensitivity studies and dynamical interpretation. *Quart. J. Roy. Meteor. Soc.,* **123,** 983–1006.

——, and ——, 1999a: The nonnormal nature of El Niño and intraseasonal variability. *J. Climate,* **12,** 2965–2982.

——, and ——, 1999b: Stochastic forcing of ENSO by the intraseasonal oscillation. *J. Climate,* **12,** 1199–1220.

Peixoto, J. P., and A. H. Oort, 1992: *Physics of Climate.* American Institute of Physics, 520 pp.

Penland, C., and P. D. Sardeshmukh, 1995: The optimal-growth of tropical sea-surface temperature anomalies. *J. Climate,* **8,** 1999–2024.

Rivin, I., and E. Tziperman, 1997: Linear versus self-sustained interdecadal thermohaline variability in a coupled box model. *J. Phys. Oceanogr.,* **27,** 1216–1232.

Sayag, R., E. Tziperman, and M. Ghil, 2004: Rapid switch-like sea ice growth and land ice-sea ice hysteresis. *Paleoceanography,* **19,** PA1021, doi:10.1029/2003PA000946.

Schmitt, R., 1994: The ocean fresh water cycle. OOSDP Tech. Rep. 4, 32 pp.

Stommel, H., 1961: Thermohaline convection with two stable regimes of flow. *Tellus,* **13,** 224–230.

Thuburn, J., and T. W. N. Haine, 2001: Adjoints of nonoscillatory advection schemes. *J. Comput. Phys.,* **171,** 616–631.

Trenberth, K. E., and J. M. Caron, 2001: Estimates of meridional atmosphere and ocean heat transports. *J. Climate,* **14,** 3433–3443.

Tziperman, E., 1997: Inherently unstable climate behaviour due to weak thermohaline ocean circulation. *Nature,* **386,** 592–595.

——, and P. J. Ioannou, 2002: Transient growth and optimal excitation of thermohaline variability. *J. Phys. Oceanogr.,* **32,** 3427–3435.

——, J. R. Toggweiler, Y. Feliks, and K. Bryan, 1994: Instability of the thermohaline circulation with respect to mixed boundary-conditions: Is it really a problem for realistic models. *J. Phys. Oceanogr.,* **24,** 217–232.

Weaver, A. J., and E. S. Sarachik, 1991: The role of mixed boundary conditions in numerical models of the ocean's climate. *J. Phys. Oceanogr.,* **21,** 1470–1493.

——, and T. M. C. Hughes, 1992: Stability and variability of the thermohaline circulation and its link to climate. *Trends Phys. Oceanogr.,* **1,** 15–69.

——, E. S. Sarachik, and J. Marotzke, 1991: Freshwater flux forcing of decadal and interdecadal oceanic variability. *Nature,* **353,** 836–838.

——, J. Marotzke, P. F. Cummins, and E. S. Sarachik, 1993: Stability and variability of the thermohaline circulation. *J. Phys. Oceanogr.,* **23,** 39–60.

Wunsch, C., 2002: What is the thermohaline circulation? *Science,* **298,** 1179–1181.

——, and R. Ferrari, 2004: Vertical mixing, energy and the general circulation of the oceans. *Annu. Rev. Fluid Mech.,* **36,** 281–314.

Zanna, L., 2003: Non-normality and optimal initial conditions of the thermohaline circulation: Physical mechanisms leading to transient growth. M.S. thesis, Weizmann Institute, Rehovot, Israel, 50 pp.